Plasmon-driven catalysis of adsorbed p-nitroaniline (PNA) by surface-enhanced Raman scattering (SERS): platinum versus silver

F.J. Vidal-Iglesias , J. Juan-Juan , I. Such-Basañez , J. Solla-Gullón , J.M. Pérez

PII: S0039-6028(19)30088-3
DOI: https://doi.org/10.1016/j.susc.2019.04.007
Reference: SUSC 21442

To appear in: *Surface Science*

Received date: 31 January 2019
Revised date: 26 April 2019
Accepted date: 30 April 2019

Please cite this article as: F.J. Vidal-Iglesias , J. Juan-Juan , I. Such-Basañez , J. Solla-Gullón , J.M. Pérez , Plasmon-driven catalysis of adsorbed p-nitroaniline (PNA) by surface-enhanced Raman scattering (SERS): platinum versus silver, *Surface Science* (2019), doi: https://doi.org/10.1016/j.susc.2019.04.007

Highlights

- A study of PNA adsorption on Pt nanoparticles is performed by SERS for the first time
- Results are discussed and compared with those published and obtained with Ag
- Similar SERS spectra were obtained on both metals when O_2 is present
- However, different SERS spectra were obtained on both metals if O_2 is absent
- Without O_2 no plasmonic catalytic reductive coupling of NO_2 group on Pt fully occurs

Plasmon-driven catalysis of adsorbed p-nitroaniline (PNA) by surface-enhanced Raman scattering (SERS): platinum versus silver

F. J. Vidal-Iglesias[a], J. Juan-Juan[b], I. Such-Basañez[b], J. Solla-Gullón[a], J. M. Pérez[a]*

[a] Instituto de Electroquímica, Universidad de Alicante, Ap 99, 03080 Alicante, Spain.

[b] SS.TT.I. Universidad de Alicante, Ap 99, 03080 Alicante, Spain.

Abstract

The adsorption of p-nitroaniline (PNA) on Pt nanoparticles, both in the absence (in aqueous solution) and in the presence of oxygen (in air environment), is studied by SERS for the first time. Differences between the plasmon-driven catalysis of adsorbed PNA on Pt and Ag nanoparticles have been found. In the presence of oxygen, the oxidative coupling of the NH_2 group in PNA to yield dinitroazobenzene (DNAB) occurs on both Pt and Ag nanoparticles. However, in the absence of oxygen, PNA behaves clearly differently on Ag than on Pt. Thus, whereas diaminoazobenzene (DAAB) is catalytically produced on Ag nanoparticles by plasmon-driven reduction reactions of the NO_2 group, on Pt nanoparticles this reaction does not fully take place as indicated by the presence of NO_2 groups on the surface of the nanoparticles. A mechanism for this distinctive behavior is tentatively proposed in which water acts as a sacrificial agent, being reduced to hydrogen by hot electrons coming from the Pt surface, while the hot holes on Pt are proposed to attach to an occupied molecular state of adsorbed PNA. The overall photocatalytic reaction of adsorbed PNA on Pt nanoparticles, in an O_2 free solution, would actually be consistent with a dehydrogenation process of water.

Keywords: SERS; p-nitroaniline; plasmon-driven catalysis; Pt nanoparticles; Ag nanoparticles.

* Corresponding author. Tel. +34 965903927.

E-mail address: jmpm@ua.es (J.M. Pérez).

Introduction

Enhanced absorption and scattering of radiation on nanoparticles results from the oscillation of free-like electrons on material surfaces excited by incident photons, the surface plasmon resonance (SPR). Interestingly, it was found that the SPR facilitated some chemical reactions [1]. The excitation of the surface plasmon in noble metal nanostructures by visible light is a very efficient process and shows excellent catalytic activity for water splitting [2-4]. In addition, it has even been observed at wavelengths as high as 1064 nm [5 6]. Particularly, plasmonic silver, gold and copper nanostructures show excellent ability for both catalytic oxidation and reduction reactions. Mukherjee et al. [7] have shown that surface plasmon excited in Au nanoparticles decays into hot electrons with energies that allow the dissociation of adsorbed H_2 on the Au nanoparticles' surface by energy transfer. Thus, they have also demonstrated that plasmon excited nanoparticles can be an efficient source of hot electrons. It is worth highlighting that plasmon-driven chemical reactions, the plasmon chemistry [8], represents an important advance in the field of nanoplasmonics. For instance, Dong et al. [9] have investigated the substrate, wavelength and time dependence of the plasmon-assisted surface catalyzed dimerization of 4-nitrobenzenethiol (4-NBT) to 4,4′-dimercaptoazobenzene (4,4′-DMAB) on Au, Ag and Cu films. In this case, they proposed the participation of hot electrons from plasmon decay, by first reducing 4-NBT by populating its LUMO orbital and then producing the dimerization. Aromatic amines [10,11] and aromatic nitro compounds [12,13] can be selectively converted to the corresponding aromatic azo compounds during SERS measurements. Interestingly, while studying 4-aminobenzenethiol (4-ABT) reaction to yield 4,4′-DMAB via SPR [14,15] it was found that the oxidative coupling of 4-ABT and reductive coupling of 4-NBT are influenced by the nature of the metal substrate, the wavelength and power of the laser employed and, when in solution, by the pH. Thus, these factors hint an important role of the environment in this photocatalytic surface reaction. Moreover, the behavior of 4-ABT has been studied on nanostructured Pt by surface-enhanced Raman scattering (SERS) and surface-enhanced infrared absorption spectroscopy (SEIRAS) [16]. In this case, it was found that different

reaction mechanisms act depending whether O_2 is present or not. When the surface reaction occurs at the gas-metal interface in the presence of a redox agent (O_2 or H_2), this agent is activated by the surface plasmon excitons reacting with adsorbed 4-ABT or 4-NBT. In this sense, participation of $^3O_2$ species has been claimed in the production of 4,4'-DMAB [17]. The role of $^3O_2$ has been investigated by SERS measurements in a $^3O_2$ free environment [18]. When this reaction occurs at the metal-liquid interface (which means absence of O_2 or H_2) 4-ABT is directly oxidized by the excited hot holes while 4-NBT is reduced by the excited hot electrons [11,19,20].

p-nitroaniline (PNA) is a chemical showing potential for use in optical disk coatings and also an important compound used as an intermediate or precursor in the manufacture of chemical agents, pesticides, pharmaceuticals, dyes, and antioxidants. This compound represents an example of typical push-pull systems that usually present large non-linear optical responses where an electron-donating group and an electron-accepting group are connected via a conjugated π system. The donor and acceptor groups provide the ground state charge asymmetry of the molecule that is necessary for second-order nonlinearity [21] which provides this molecule with interesting properties as a non-linear optic material [22,23]. SEIRAS and SERS techniques have been used by Posey et al. [24] to study the adsorption behavior of nitroaniline isomers on silver surfaces in a non-electrochemical environment (both on vacuum-deposited silver films and on silver powders). Moreover, the adsorption of PNA on silver and gold electrodes in aqueous and non-aqueous media has been studied by SERS [25-29]. Interestingly, Zhao et al [30] have studied the effect of the surroundings on the reaction route of the plasmonic photocatalysis of PNA on silver substrates. From DFT calculations they suggest that PNA may undergo two possible reaction routes: i) the oxidative coupling of amino groups to dinitroazobenzene (DNAB), rather than nitroaminoazobenzene (NAAB), and ii) the reductive coupling of nitro groups to diaminoazobenzene (DAAB). More recently, Ding et al [31] have studied by SERS the plasmon-driven diazo coupling reaction of PNA, under atmospheric environment, on both Ag nanoparticles and graphene-modified Ag substrates (nanoparticles and

nanowires). They found that PNA was converted (selective dimerization reaction) into DAAB rather than oxidized into DNAB. Similarly, under electrochemical control, SERS studies have reported that the reduction of the nitro group on Ag electrodes is much easier than other oxidation reactions [8,14]. It is worth noting that plasmon-driven multiple-steps surface catalytic reactions can also take place. Sun et al. [32] observed that p-dinitrobenzene (PDNB) was reduced to DAAB via double reduction reaction, that is, PDNB is firstly reduced to DNAB, and then further reduced to DAAB in a two-step reduction reaction. Very recently, Sun et al. [33] reported an interesting contribution reviewing some recent findings on “electricity stimulated” plasmon-driven surface catalysis monitored by electrochemical SERS spectroscopy in aqueous environments not only including relevant plasmon-driven reduction and oxidation catalytic reactions but also the influence of some parameters such as laser intensity, potential, pH and local SPR factors. Interestingly, this review also pointed out the application of plasmon−exciton coupling co-driven surface catalytic reactions on plasmonic metal−graphene hybrid for both reduction and oxidation reactions [33-36].

To the best of our knowledge, the adsorption of PNA on Pt has been scarcely investigated despite the importance of this transition metal as catalytic and electrocatalytic material. In this regard, and even considering the non-efficient excitation of its surface plasmon, an adequate surface morphology can be tailored by suitable methods (among them oxidation–reduction cycling [37] and nanoparticle-on-electrode approach [38]) in order to obtain SERS spectra from these metals. In this manuscript, we perform, for the first time, a SERS study of the adsorption behavior of PNA on Pt nanoparticles, both in the absence (deoxygenated aqueous solution) and in the presence of O_2 (in air environment). The results obtained are discussed and compared with those obtained by using Ag nanoparticles. Energy levels of the different species taking part in the reaction are calculated by DFT methods and could help the observed behavior of adsorbed PNA on Pt to be explained.

Experimental details

Synthesis of nanostructures.

The synthesis of the Pt and Ag nanostructures was performed using a methodology similar to that described in previous contributions [15,19, 33]. Very briefly, 20 mL of an aqueous solution of the metallic precursor containing 2.5×10^{-4} M H_2PtCl_6 (Aldrich, 99.999%) or 2.5×10^{-4} M $AgNO_3$ (Panreac, 99%) and 2.5×10^{-4} M trisodium citrate (Sigma-Aldrich, ≥ 99.0%) was prepared in a glass beaker at room temperature. Then, 0.6 mL of an ice-cold and freshly prepared 0.1 M $NaBH_4$ (Aldrich, 99%) solution was added to the solution under vigorous stirring. After 30 s the stirring was stopped, and the solution was kept unperturbed for at least 30 min. It is well-accepted that the use of surface cleaned (organics free) nanostructures is a relevant aspect for studying electrocatalytic reactions. The cleaning of these samples (removal of the citrate molecules acting as capping agent and attached to the surface of the nanostructures) was performed using the so-called *alkaline treatment* as described in previous contributions [39-41]. In brief, a NaOH (Merck, p.a.) pellet (~0.2 g) was directly added to each colloidal solution. The incorporation of the NaOH gives rise to the destabilization of the colloid and, consequently, to the precipitation of the nanostructures. After complete precipitation, the nanostructures were washed 3−4 times with ultrapure water. TEM experiments were performed with a JEOL JEM 2010 microscope working at 200 kV. The sample for TEM analysis was obtained by placing a drop of the water suspension containing the clean nanostructures onto a Formvar-covered copper grid and evaporating the solvent in air at room temperature.

Electrochemical measurements.

Electrochemical measurements were performed at room temperature in 0.1 M $KClO_4$ or 0.1M $KClO_4$ + 10^{-3} M PNA solutions. Working solutions were daily prepared from Millipore Milli-Q water (18.2 MΩ·cm), potassium perchlorate (Merck, p.a.) and PNA (97% Aldrich). Solutions were deaerated with Ar (N50, Air Liquide). A three-electrode electrochemical cell was used. The electrode

potential was controlled using a PGSTAT302N AUTOLAB system. An Au wire was used as counter electrode and a polyoriented Pt or Ag bead electrode as working electrode. The working electrodes were flame annealed before being employed in the electrochemical cell. Potentials were measured against a AgCl/Ag reference electrode connected to the cell through a Luggin capillary.

Computational details.

All calculations were performed by using DFT B3LYP functional as implemented in the Gaussian 09 code [42]. For the analysis of vibrational modes of the isolated reactant and product molecules, a triple-ζ correlation consistent basis set cc-pVTZ was used. The frequencies were scaled using 0.965 factor. No imaginary frequencies were observed in any of the calculations presented in this work. The assignment of the Raman bands of DAAB, DNAB and NAAB were also supported by calculated vibrational frequencies. Visualization of structures and vibrational normal modes was performed by using Avogadro 1.1 Software [43]. A flat Pt(111) metal cluster surface, comprising 15 atoms arranged in two layers (10 and 5 atoms, respectively) was used for calculating HOMO-LUMO energies of different molecules adsorbed on platinum. All platinum atoms were kept fixed in the bulk metal theoretical positions. The platinum atoms were described using a LANL2DZ effective core potential, while a 6-31G(d,p) basis set was considered for atoms in the adsorbed molecules. Adsorption of PNA on the metal cluster through the NO_2 group was considered, as suggested in previous studies [30, 44]. Associative adsorption of water through the oxygen atom, and associative adsorption of oxygen molecules were studied in accordance with related studies [30]. The adsorbed molecules were allowed to relax on the metal surface until a local minimum was found.

SERS measurements.

SERS measurements were performed using the so-called nanoparticles-on-electrode approach [38,45,46]. The Ag and Pt nanostructured electrodes

were made by depositing a droplet of the corresponding metal nanostructure aqueous suspension onto a polycrystalline polished Ag or Pt disk (3 mm in diameter) sheathed in a threaded poly-(tetrafluoroethylene) (PTFE) piece by using a pipette. The droplet was dried in air and the substrate was then mounted on a PTFE flow cell specifically designed for the *in situ* Raman measurements. In electrochemical environments, a saturated AgCl/Ag electrode was used as a reference electrode and a Pt wire was used as counter electrode. Raman spectra were obtained with a NRS-5000 laser Raman spectrometer (Jasco). Two excitation lines were used: a 50 mW Nd:YAG laser at 532 nm and a 17 mW He−Ne laser at 632.8 nm. The laser beams were focused through a 50×LWD objective (0.5 NA) into a 2 μm spot at the electrode surface. The spectrometer resolution was better than 5 cm^{-1} and the detector was a Peltier cooled charge coupled device (CCD) (1024 × 256 pixels).

Results and discussion

Figures 1a and 1b show some representative TEM images of the Ag and Pt nanostructures used in this work, respectively. As previously discussed in ref [47], the removal of the citrate molecules surrounding the colloidal Ag nanoparticles (about 6 nm) produces an evident agglomeration and sintering, giving rise to aggregated Ag nanostructures as illustrated in figure 1a. However, this cleaning procedure does not affect the Pt nanoparticles (about 3 nm), which remain essentially unchanged (in terms of particle size and shape) as shown in figure 1b.

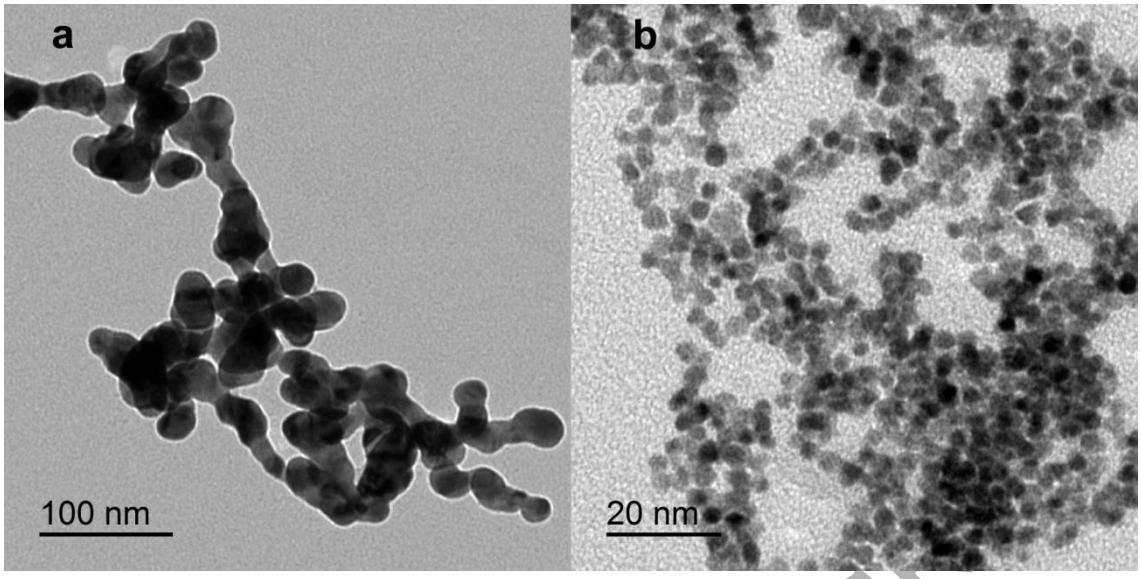

Figure 1

Figure 2 displays the voltammetric response of polyoriented Pt (figure 2a) and Ag (figures 2b and 2c) bead electrodes in 0.1 M $KClO_4$ solution in the absence (black lines) and presence (red lines) of 10^{-3} M PNA. In the case of Pt, the voltammogram obtained in the presence of PNA is essentially similar to that previously reported by Jbarah and Holze [48] obtained with a platinum-sheet in a PNA saturated 0.1 M $KClO_4$ solution. This voltammogram shows a reduction process at about -0.8 V vs AgCl/Ag together with the incipient hydrogen evolution reaction (HER). In addition, an oxidation process at about 0.06 V and a wide reduction contribution (centered at about -0.28 V) are also observed. The voltammetric response for Ag is even more complex and presents a defined reduction process at about -0.52 V (well-separated from the HER on Ag which occurs at about -1.1 V and related to the reduction of the nitro group to a hydroxylamine group (–NHOH)) together with a redox reversible couple at about -0.14 and -0.06 V. In addition, two poorly defined anodic contributions and one cathodic process are observed at positive potential just before the incipient Ag oxidation. This complex response displays some similarities with that obtained with gold-sheet electrodes in PNA saturated 0.1 M $KClO_4$ solution [42] except for the redox reversible couple at about -0.14 and -0.06 V, which is not observed for gold at this pH. Based on previous contributions, Jbarah and Holze suggested that the oxidation and reduction processes observed in the positive potential region could be assigned to the oxidation of p-amino-N-

phenylhydroxylamine and p-phenylenediamine (p-PDA) and to the reduction of p-nitroaniline which is formed through a homogeneous reaction. However, as they finally stated, a convenient assignment of these contributions is as yet impossible [48]. About the redox reversible couple at -0.14 and -0.06 V, Jbarah and Holze found similar redox features at lower pH (PNA saturated 0.1 M $HClO_4$ solution), which were attributed to a reversible oxidation of amino groups of the p-PDA formed by the electrochemical reduction of PNA through an ECE (electron transfer, chemical reaction, electron transfer) mechanism [48]. Nonetheless, Zavar et al. [49] suggested that the redox couple could be related to a reversible two-electron oxidation reduction of the hydroxylamine group (–NHOH) to a nitroso group (–NO).

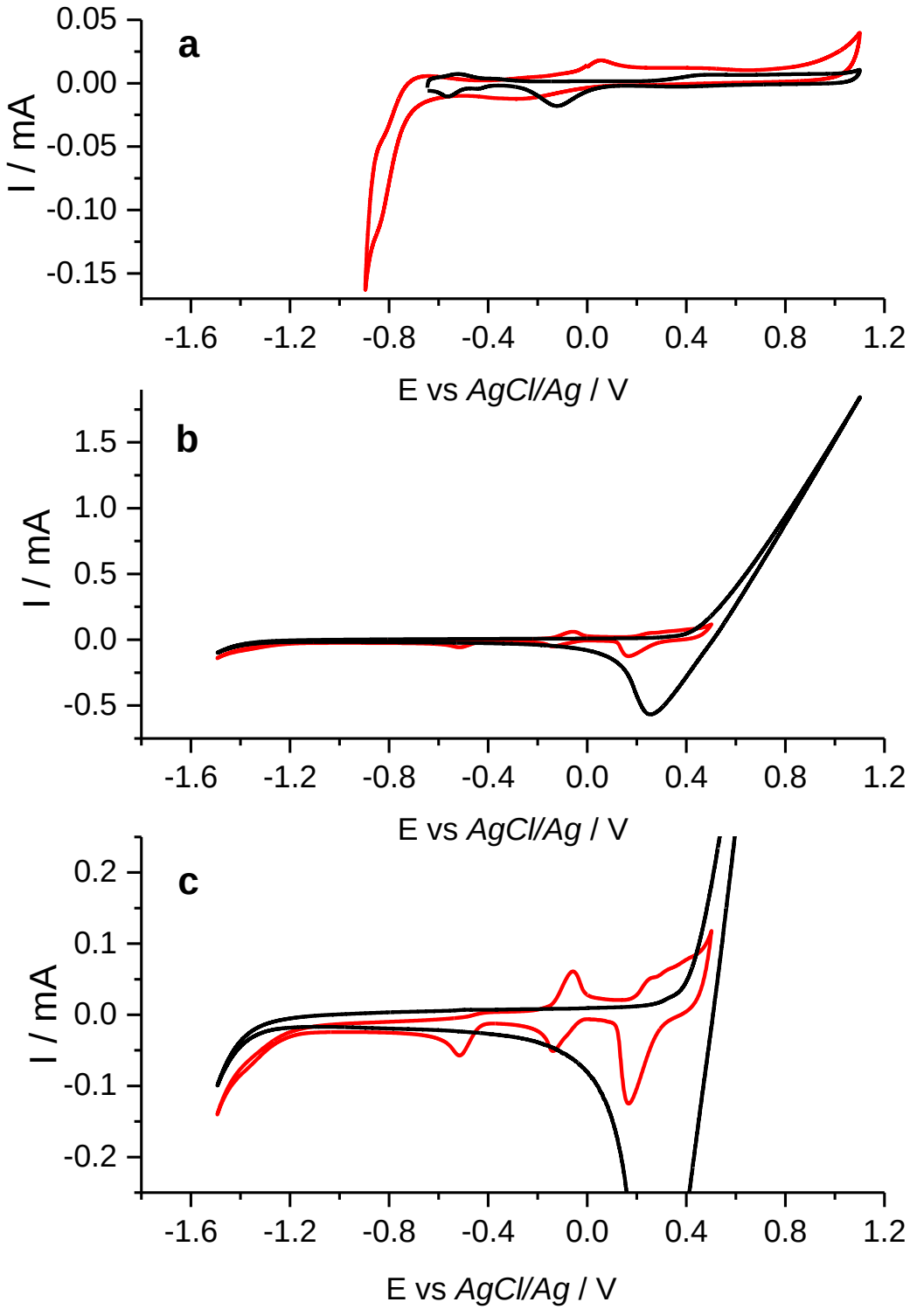
a
0.05
0.00
-0.05
-0.10
-0.15
I / mA
-1.6
-1.2
-0.8
-0.4
0.0
0.4
0.8
1.2
E vs AgCl/Ag / V
b
1.5
1.0
0.5
0.0
-0.5
I / mA
-1.6
-1.2
-0.8
-0.4
0.0
0.4
0.8
1.2
E vs AgCl/Ag / V
c
0.2
0.1
0.0
-0.1
-0.2
I / mA
-1.6
-1.2
-0.8
-0.4
0.0
0.4
0.8
1.2
E vs AgCl/Ag / V

Figure 2

Figure 3a shows the Raman spectrum of solid PNA with main bands at 1110, 1180, 1280, 1315, 1337, 1394, 1450, 1507, 1590 and 1630 cm^{-1}. The most intense band (1280 cm^{-1}) is attributed to the $\nu[C\text{-}NH_2] + \delta[CH]$ vibration, while the band at 1337 cm^{-1} is assigned to $\nu[C\text{-}NO_2] + \delta[CH]$ [27,44]. Figures 3(b-f), show SERS spectra of PNA adsorbed on Ag in a (0.1 M $KClO_4$ + 1mM PNA) deoxygenated solution, at different electrode potentials, and obtained with a 532 nm laser. These spectra display a different set of bands at 1145, 1200, 1317, 1405, 1450, 1503, 1598 and 1607 cm^{-1}. These results agree with those previously reported by Cui et al. [8]. The appearance of new bands in the SERS spectra of PNA adsorbed on nanostructured Ag is a proof that plasmon-driven chemical reactions are occurring through the amine and/or nitro groups of adsorbed PNA during the spectral acquisition. There are numerous cases in the literature where changing SERS spectra indicate that some sort of photochemical process is occuring as spectra are acquired. Furthermore, reactions between “hot” excited metallic electrons and adsorbed molecules in electrochemical junctions and on high vacuum surfaces are often observed [50,51]. In addition, it has been reported that DAAB can be catalytically produced by plasmon-driven reduction of the NO_2 group in PNA when O_2 is absent [8,30], as occurs in a deoxygenated solution.

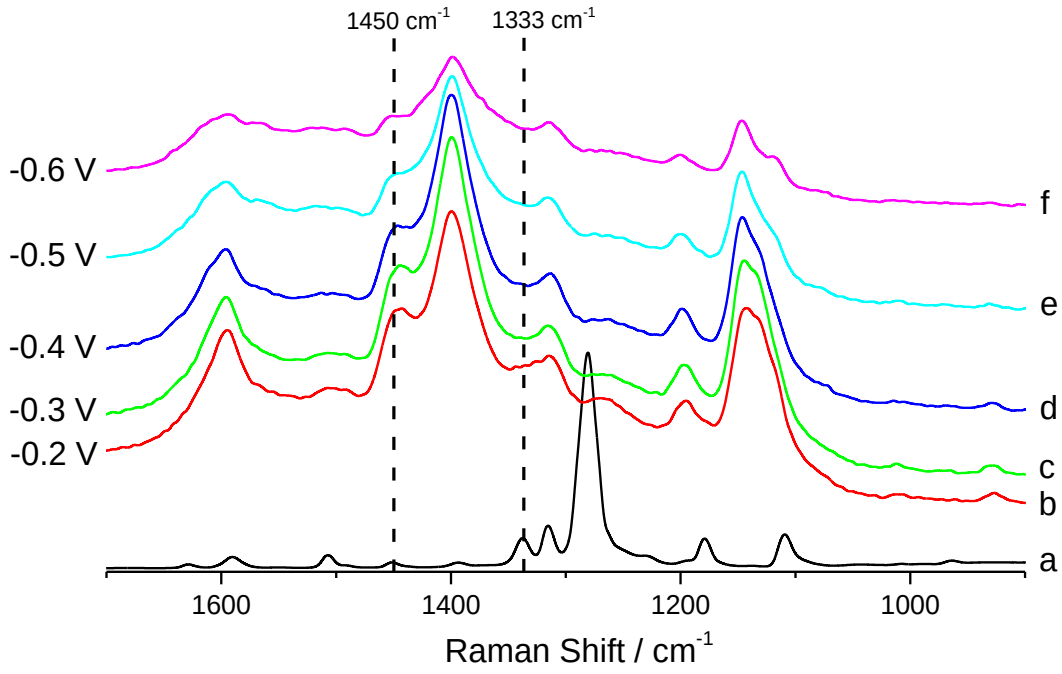

Figure 3

On the other hand, Posey et al. [24] have reported that, in the presence of O_2, the SERS spectrum of PNA deposited on a silver film, obtained with a 632.8 nm laser, presents several bands assigned to the NO_2 group. In this sense, a theoretical study [30] focusing on the effect of the environment on the reaction route of the plasmonic photocatalytic reaction of PNA, reported that, in the presence of O_2, the plasmon-driven oxidation reaction via the amine group should be favored against the plasmon-driven reduction reaction via the nitro group. However, more recently, Ding et al [31] experimentally found that, in atmosphere environment, PNA was transformed selectively into DAAB on Ag nanoparticles. To better visualize the effect of the presence or absence of O_2, figure 4 shows the SERS spectra obtained with the 532 nm laser of PNA deposited on nanostructured Ag, both in deoxygenated solution, taken at 0.2 V vs AgCl/Ag, and in air. For the sake of comparison, the Raman spectrum of commercially available DAAB is also included. It can be observed that the DAAB spectrum reproduces well the SERS spectrum of PNA on Ag in deoxygenated solution. According to that, DAAB is being catalytically produced by plasmon-driven reduction reactions of NO_2 group in PNA. However, in the presence of O_2, a band at 1333 cm^{-1}, assigned to $\nu_s(NO_2)$, is clearly visible. Therefore, when O_2 is present, the plasmon-driven reduction reaction of NO_2

group does not occur completely. Similar findings are obtained when the 632.8 nm laser is used, independently of the relative intensities of the bands (see supporting information, Figure S1). It is worth noting that the spectrum obtained in this work using the 632.8 nm laser in an ambient environment matches the one reported by Posey et al. [24] and the results agree with those previously published [14,30].

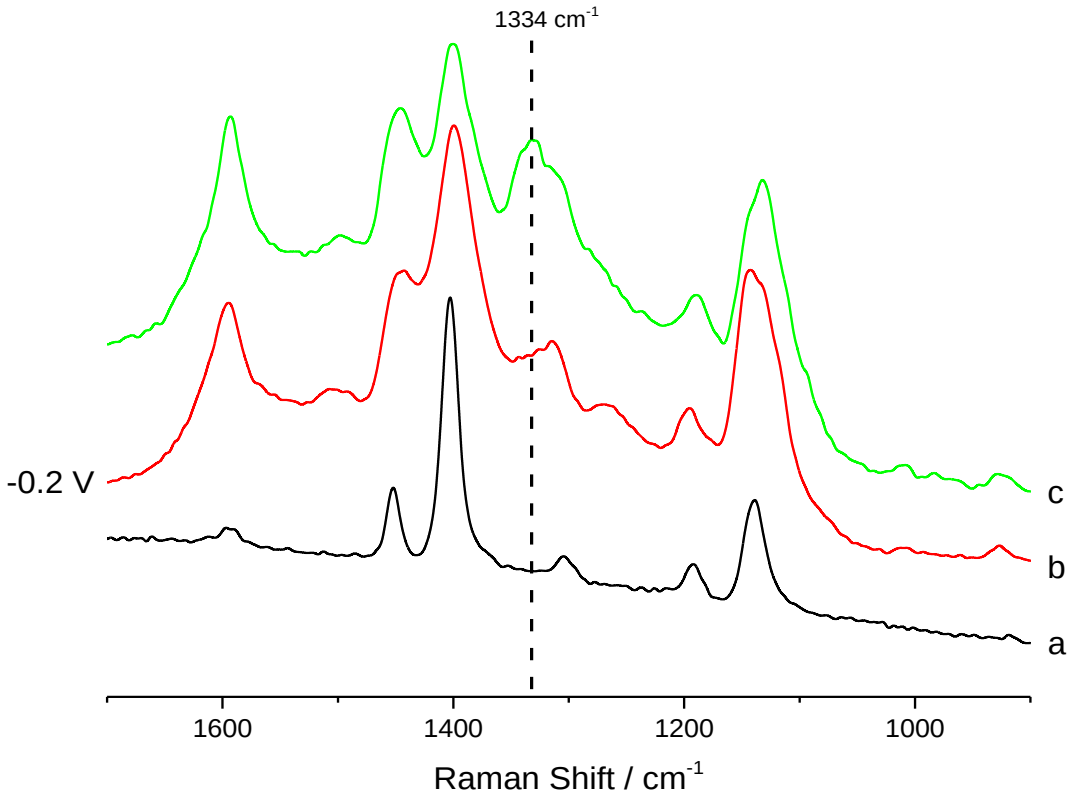

Figure 4

To complete this analysis, Figure 5 reports the spectra of adsorbed PNA in the presence and in the absence of O_2, together with the experimental spectra of DAAB and the calculated spectra of DAAB, NAAB and DNAB. As indicated in Table 1, the band corresponding to the $\nu_s(NO_2)$, which appears when O_2 is present, is only predicted in the DNAB and NAAB calculated spectra. Previously reported DFT calculations [30] concluded that when PNA and oxygen are co-adsorbed on a silver surface, oxygen is first activated by the excited hot electrons, and the hydrogen atoms in the amino group of PNA are

successively removed by this active oxygen species. Consequently, when oxygen is present, adsorbed PNA on Ag should be mainly transformed into DNAB (rather than NAAB) through a catalyzed oxidative coupling reaction during the SERS experiment.

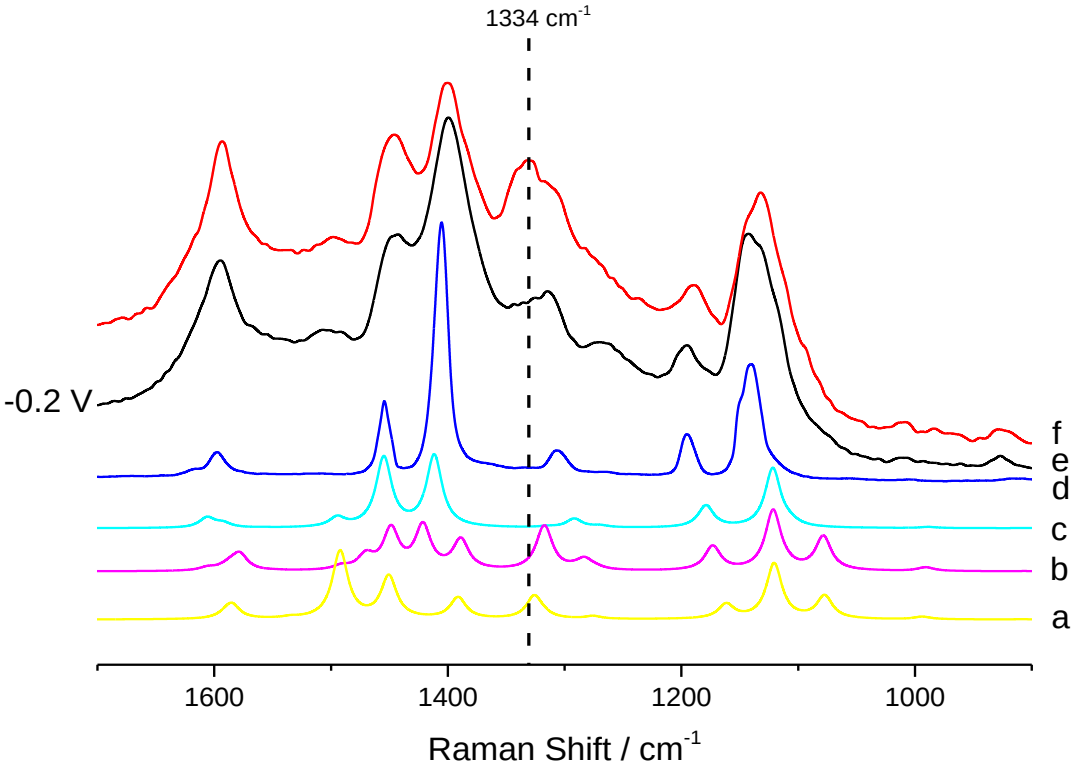

Figure 5

Moving forward to the case of Pt, Figure 6 (d-g) shows the spectra of PNA adsorbed on Pt in aqueous solution (0.1 M $KClO_4$ + 1mM PNA), obtained in absence of O_2 at different electrode potentials and with the 632.8 nm laser. These spectra are characterized by a set of bands at 1112, 1167, 1333, 1387, 1517 and 1598 cm^{-1}. Similar spectra (in this case also in terms of relative intensities) are recorded with the 532 nm laser (see supporting information, Figure S2). Again, the appearance of new bands in the SERS spectra suggests the existence of a photocatalytic process on Pt. Table 1 summarizes the wavenumbers (cm^{-1}) and assignments of the observed bands in the SERS spectra of adsorbed PNA on Ag and Pt nanoparticles in a deoxygenated

solution and in air environment also including those in the Raman spectrum of PNA in its solid form, together with the experimental spectrum of DAAB and the calculated spectra of DAAB, NAAB and DNAB. Some differences between the SERS spectra of PNA adsorbed on Ag and Pt in a deoxygenated solution can be pointed out. It is apparent that in the case of Pt a band at 1333 cm^{-1} (assigned to the presence of NO_2 group on the surface) is clearly observed in these spectra in the range of potentials studied while this band is absent in the case of Ag. On the other hand, the bands at 1112 and 1167 cm^{-1} are red-shifted by about 33 cm^{-1} compared to those of Ag. Similar results were obtained using more diluted PNA solution (10^{-5} M, see supporting information, Figure S3).

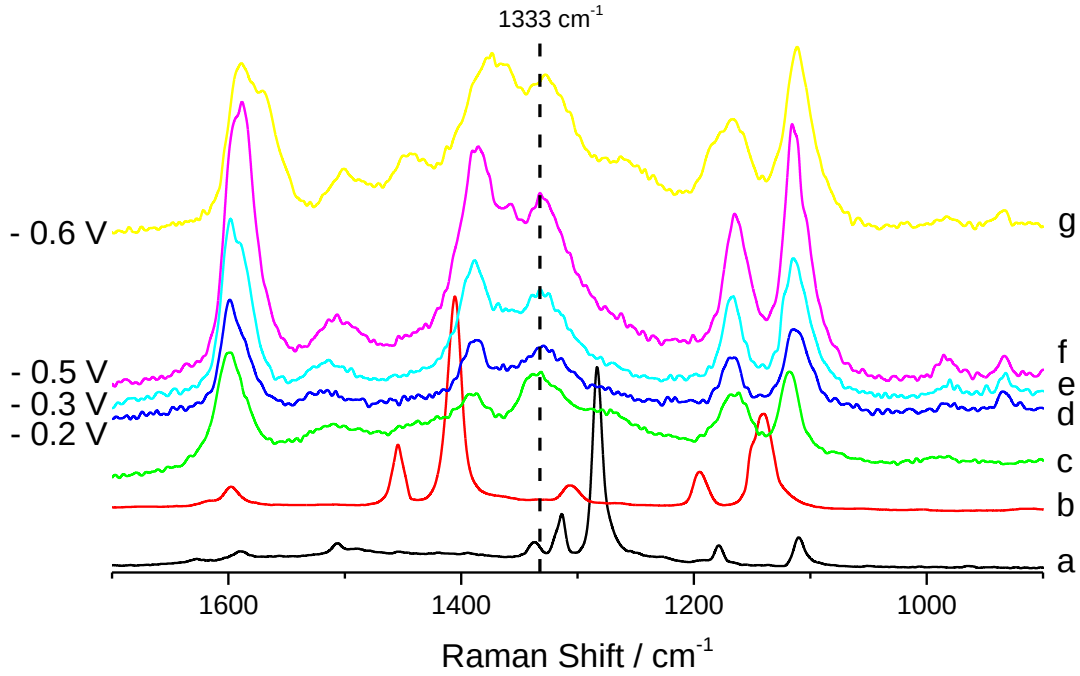

Figure 6

Surprisingly, when a nanostructured Pt is used as active SERS substrate, the spectra in the presence (figure 6c) or in the absence (figures 6(d-g)) of O_2 do not show any significant difference. For the sake of comparison, the spectra of PNA and DAAB, figures 6a and 6c, respectively, are also included. It can be observed that the DAAB spectrum does not fit with the spectrum of PNA adsorbed on Pt in the presence of O_2 (in air). This finding suggests that the plasmon-driven reduction via the nitro group does not occur or at least does not

reach completeness, independently of the presence or absence of O_2. The SERS spectra of PNA on Pt agree quite well with the calculated Raman spectrum of DNAB and the experimental spectra of DNAB reported by Cui et al. [14]. Equivalent results are obtained by using the 532 nm laser (see supporting information, Figure S2). Thus, unlike silver, the plasmon-driven reaction of PNA on Pt would produce as a major product DNAB (rather than DAAB), with both 532 nm and 632.8 nm lasers, independently whether or not O_2 is present. This fact may be an indication that a competitive mechanism of both plasmon-driven reactions (oxidation and reduction) would take place on Pt.

In order to explain the behavior of PNA on Pt, the calculated HOMO and LUMO energy levels of PNA adsorbed on Pt together with its Fermi level are shown in Figure 7. The energy gap between LUMO and HOMO for PNA adsorbed on Pt is about 0.75 eV while in the case of silver is close to 4 eV [30]. As mentioned before, the non-radiant decay of surface plasmon yields hot electron-hole pairs. The excited electrons and holes can be transferred to the chemisorbed species assuming that a suitable acceptor level is available. In the case of silver, it was concluded that the hot electrons were more likely to transfer to the LUMO of adsorbed oxygen than to the LUMO of adsorbed PNA [30]. Consequently, the surface plasmon-mediated hot electron injection to the antibonding orbital of adsorbed oxygen will dissociate the oxygen molecules located close to the silver surface. Similarly, when PNA and oxygen are coadsorbed on a Pt surface, the transfer of hot electrons to the LUMO of adsorbed oxygen will also be more likely than to the LUMO of adsorbed PNA. In this way, surface plasmon-mediated hot electron injection to the antibonding orbital of adsorbed oxygen will dissociate the oxygen molecules located close to the platinum surface. As the activated surface oxygen species have a very strong oxidation capability, it can consecutively extract hydrogen atoms of two nearby PNA molecules to yield DNAB molecules.

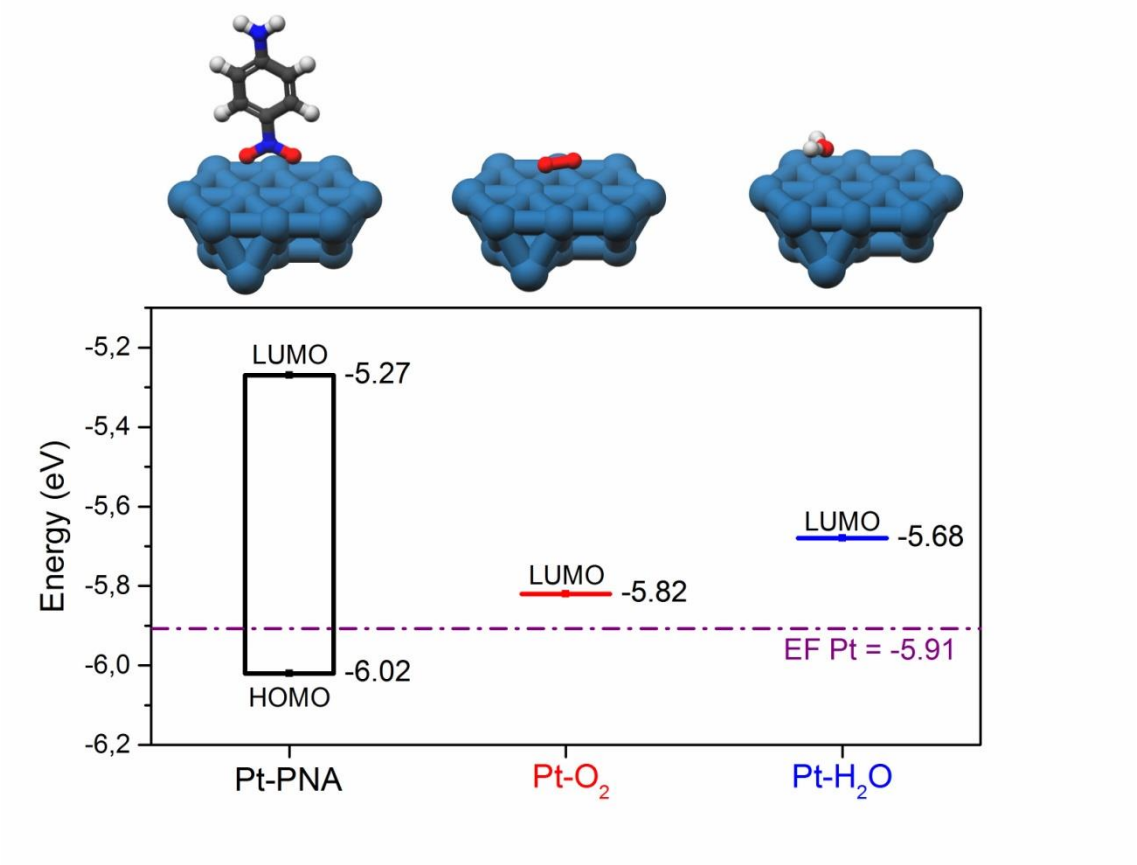

Figure 7

As previously discussed, in contrast with the case of silver, similar SERS spectra are obtained with Pt both in the presence and in the absence of O_2 (Figure 6). Thus, no plasmonic catalytic reductive coupling to produce DAAB seems to occur in its entirety over Pt under any conditions. In a free O_2 solution, water is now proposed as a sacrificial agent. It is well established that Pt is a much better electrocatalyst for HER than silver [52-54]. In fact, Pt is the best-known catalyst for HER and only requires a very small overpotential to drive the hydrogen evolution reaction. In contrast, Ag displays a poor HER activity which can be easily understood on the basis of the prediction of the volcano plots according to their positive ΔG(M-H). In addition, as occurs with oxygen, the LUMO level of adsorbed water (-5.68 eV) is lower than that of adsorbed PNA (-5.27 eV). Water molecules approaching the platinum surface will then be activated and dissociated through the surface plasmon-mediated hot electron injection to the antibonding orbital of water. In this way, water molecules should be reduced by the hot electron to generate hydrogen [55-57]. Thus, the hot hole

in the metal substrate is proposed to attach to an occupied molecular state of adsorbed PNA [58]. A similar mechanism has been also claimed to explain the conversion of 4-ABT to 4,4'-DMAB via oxidation by the hot hole, while water is reduced as a sacrificial agent by the hot electron to release hydrogen [11,20,59,60]. In consequence, the overall reaction of photocatalysis of adsorbed PNA on Pt in a free O_2 solution would actually be a dehydrogenation process, particularly the dehydrogenation of water.

Conclusions

The adsorption of PNA on Ag and Pt substrates by spectroelectrochemical measurements has been studied. When oxygen is present (in air) similar SERS spectra are obtained when PNA is adsorbed on both metals. In this case, oxidative coupling of amino group by the activated oxygen produced by excited hot electrons yields mainly DNAB. However, in the absence of oxygen, and in contrast with what occurs on Ag, no plasmonic catalytic reductive coupling of NO_2 group to yield DAAB seems to occur in its entirety on Pt. This is revealed by the presence of characteristic bands of NO_2 groups in the range of potentials studied. Calculated energy levels of the different species taking part help to explain the behavior of adsorbed PNA on Pt in the absence of oxygen. In addition, water is proposed as a sacrificial agent being reduced by the hot electron to produce hydrogen. Under these conditions, water molecules approaching the platinum surface will be activated and then dissociated through the surface plasmon-mediated hot electron injection to the antibonding orbital of water. Subsequently, the hot hole in Pt would interact with an occupied molecular state of adsorbed PNA. As a consequence, in a free O_2 solution, the overall reaction of photocatalysis of adsorbed PNA on Pt nanoparticles would be in fact the dehydrogenation of water.

Acknowledgments

This work was conducted under the framework of the Spanish Ministry of Economy, Industry and Competitiveness (MINECO), project CTQ2016-76231-

C2-2-R (AEI/FEDER, UE). JSG acknowledges financial support from VITC (Vicerrectorado de Investigación y Transferencia de Conocimiento) of the University of Alicante (UATALENTO16-02).

Table 1. Spectral data for PNA (cm^{-1}) as a solid and adsorbed on Ag (532 nm laser) and Pt (632.8 nm laser) nanoparticles in a deoxygenated solution and in air environment, together to those of DAAB, DNAB and NAAB.

	PNA (s)		PNA(Ag)[a]	PNA(Ag)[b]	PNA(Pt)[a,b]	DAAB(exp)	DAAB(cal)	DNAB(cal)	NAAB(cal)
δ(CH)+ν(C-NO_2)	1110	δ(CH)+ν(C-NO_2)	------	1116	1112	------	------	1077	1078
	------	δ(CH)+ν(C-N)	1145	------	------	1140	1121	1120	1121
δ(CH)	1180	δ(CH)+ν(C-N)	------	1164	1167	------	------	1161	1173
			1200	------	------	1193	1180		
δ(CH)+δ(NH_2)	1280		------	------	------	------	------	------	------
ν(ring)	1315	β_{as}(CH)	1317	------	------	1314	1292	------	1283
ν(C-NO_2)+δ(CH)	1337	ν_s(NO_2)	------	1334	1333	------	------	1325	1318
ν(C-NH_2)	1394	δ(CH)+ν(N=N)	1405	1390	1387	1403	1411	1391	1389
ν(ring)	1450	ν(ring)+ν(N=N)	1450	1451	1450(*)	1453	1454	1450	1450
ν(ring)	------	ν(N=N)+β_{as}(CH)	------	------	------	------	------	------	1470
ν(ring)	1507	ν(N=N)+β_{as}(CH)	1503	1514	1517	------	1494	1492	1491
ν(ring)	1590	ν(N=N)+ν(ring)	1598	1598	1598	1597	1592	1585	1584
β_s(NH_2)	1630	δ(NH_2)+ν(C=C)	1607	------	------	1612	1606	------	1606

a) (0.1 M $KClO_4$ + 1mM PNA) deoxygenated solution; b) air environment; (*) very weak at 10^{-3}M and clearly visible at 10^{-5} M (see Figure S3)

δ, in-plane deformation; ν, stretching; β_{as}, rocking; β_s, scissoring

References

[1] K. M. Mayer, J. H. Hafner, Localized surface plasmon resonance sensors. Chem. Rev. 111, (2011), 3828-3857.

[2] C. Gomes Silva, R. Juárez, T. Marino, R. Molinari, H. García, Influence of Excitation Wavelength (UV or Visible Light) on the Photocatalytic Activity of Titania Containing Gold Nanoparticles for the Generation of Hydrogen or Oxygen from Water. J. Am. Chem. Soc. 133, (2010), 595−602.

[3] D. B. Ingram, S. Linic, Water Splitting on Composite Plasmonic-Metal/Semiconductor Photoelectrodes: Evidence for Selective Plasmon-Induced Formation of Charge Carriers Near the Semiconductor Surface. J. Am. Chem. Soc. 133, (2011), 5202−5205.

[4] S. Navalon, M. de Miguel, R. Martin, M. Alvaro, H. Garcia, Enhancement of the Catalytic Activity of Supported Gold Nanoparticles for the Fenton Reaction by Light. J. Am. Chem. Soc. 133, (2011), 2218−2226.

[5] Y. Nishijima, K. Ueno, Y. Yokota, K. Murakoshi, H. Misawa, Plasmon-Assisted Photocurrent Generation from Visible to Near-Infrared Wavelength Using an Au-Nanorods/TiO2 Electrode. J. Phys.Chem. Lett. 1, (2010), 2031−2036.

[6] Z. Mao, W. Song, L. Chen, W. Ji, X. Xue, W. Ruan, Z. Li, H. Mao, S. Ma, J.R. Lombardi, et al. Metal−Semiconductor Contacts Induce the Charge-Transfer Mechanism of Surface-Enhanced Raman Scattering. J. Phys. Chem. C 115, (2011), 18378−18383.

[7] S. Mukherjee, F. Libisch, N. Large, O. Neumann, L. V. Brown, J. Cheng, J. B. Lassiter, E. A. Carter, P. Nordlander, N. J. Halas, Hot Electrons Do the Impossible: Plasmon-Induced Dissociation of H_2 on Au. Nano Lett. 13, (2013), 240−247.

[8] L. Cui, P. Wanh, Y. Li, M. Sun, Selective plasmon-driven catalysis for para-nitroaniline in aqueous enviroments. Sci. Rep.6, (2016), 20458.

[9] B. Dong, Y. Fang, X. Chen, H. Xu, M. Sun, Substrate-, Wavelength-, and Time-Dependent Plasmon-Assisted Surface Catalysis Reaction of 4-Nitrobenzenethiol Dimerizing to *p,p'*-Dimercaptoazobenzene on Au, Ag, and Cu Films. Langmuir 27, (2011), 10677−10682.

[10] D. Y. Wu, X. M. Liu, Y. F. Huang, B. Ren, X. Xu, Z. Q. Tian, Surface Catalytic Coupling Reaction of *p*-Mercaptoaniline Linking to Silver Nanostructures Responsible for Abnormal SERS Enhancement: A DFT Study. J. Phys. Chem. C 113, (2009), 18212– 18222.

[11] L. B. Zhao, M. Zhang, Y. F. Huang, C. T. Williams, D. Y. Wu, B. Ren, Z. Q. Tian, Theoretical Study of Plasmon-Enhanced Surface Catalytic Coupling

Reactions of Aromatic Amines and Nitro Compounds. J. Phys. Chem. Lett. 5, (2014), 1259– 1266.

[12] B. Dong, Y. Fang, X. Chen, H. Xu, M. Sun, Substrate-, Wavelength-, and Time-Dependent Plasmon-Assisted Surface Catalysis Reaction of 4-Nitrobenzenethiol Dimerizing to *p,p′*-Dimercaptoazobenzene on Au, Ag, and Cu Films. Langmuir. 27, (2011), 10677–10682.

[13] W. Xie, C. Herrmann, K. Kömpe, M. Haase, S. Schlücker, Synthesis of Bifunctional Au/Pt/Au Core/Shell Nanoraspberries for in Situ Sers Monitoring of Platinum-Catalyzed Reactions. J. Am. Chem. Soc. 133, (2011), 19302–19305.

[14] L. Cui, P. Wang, Y. Fang, Y. Li, M. Sun, A plasmon-driven selective surface catalytic reaction revealed by surface-enhanced Raman scattering in an electrochemical environment. Sci. Rep. 5, (2015), 11920.

[15] Y. Fang,Y. Li, H. Xu, M. Sun, Ascertaining *p,p'*-Dimercaptoazobenzene Produced from *p*-Aminothiophenol by Selective Catalytic Coupling Reaction on Silver Nanoparticles. Langmuir 26, (2010), 7737-7746.

[16] F. J. Vidal-Iglesias, J. Solla-Gullón, A. Rodes, J. M. Feliu, J. M. Pérez, Spectroelectrochemical behavior of 4-aminobenzenethiol on nanostructured platinum and silver electrodes. Surf. Sci. 631, (2015), 213–219

[17] P. Xu, L. Kang, K.S. Mack, K.S. Schanze, X. Han, H.L. Wang, Mechanistic understanding of surface plasmon assisted catalysis on a single particle: cyclic redox of 4-aminothiophenol. Sci. Rep. 3, (2013), 2997.

[18] Y. F. Huang, M. Zhang, L. B. Zhao, J. M. Feng, D. Y. Wu, B.; Ren, Z. Q. Tian, Activation of Oxygen on Gold and Silver Nanoparticles Assisted by Surface Plasmon Resonanaces. Angew. Chem. Int. Ed. 53, (2014), 2353-5357.

[19] L. B. Zhao, Y. F. Huang, X. M. Liu, J. R. Anema, D. Y. Wu, B. Ren, Z.Q. Tian, A DFT Study on Photoinduced Surface Catalytic Coupling Reactions on Nanostructured Silver: Selective Formation of Azobenzene Derivatives from Para-Substituted Nitrobenzene and Aniline. Phys. Chem. Chem. Phys**.** 14, (2012), 12919–12929.

[20] F. J. Vidal-Iglesias, J. Solla-Gullón, J. M. Orts, A. Rodes, J. M. Pérez, Spectroelectrochemical Study of the Photoinduced Catalytic Formation of 4,4′-Dimercaptoazobenzene from 4-Aminobenzenethiol Adsorbed on Nanostructured Copper. J. Phys. Chem. C. 119, (2015), 12312−12324.

[21] F. L. Huyskens, P. L. Huyskens, A. P. Persoons, Solvent dependence of the first hyperpolarizability of p-nitroanilines: Differences between nonspecific dipole-dipole interactions and solute-solvent H-bonds. J. Chem. Phys. 108, (1998), 861-8171.

[22] J. Hu, B. Zhao, W. Xu, Y. Fan, B. Li, Y. Ozaki, Aggregation of silver particles trapped at an air-water interface for preparing new SERS active substrates. J. Phys. Chem. B 106, (2002), 6500-6506.

[23] J. Hu, B. Zhao, W. Xu, Y. Fan, B. Li, Y. Ozaki, Simple method for preparing controllably aggregated silver particle films used as surface-enhanced Raman scattering active substrates. Langmuir 18, (2002), 6839-6844.

[24] K. L. Posey, M. G. Viegas, A. J. Boucher, C. Wang, K. R. Stambaugh, M. M. Smith, B. G. Carpenter, B. L. Bridges, S. E. Baker, D. A. Perry, Surface-Enhanced Vibrational and TPD Study of Nitroaniline Isomers. J. Phys. Chem. C 111, (2007), 12352-12360.

[25] R. Holze, The Adsorption of *p*-Nitroaniline on Silver and Gold electrodes as Studied with Surface Enhanced Raman Spectroscopy (SERS). Electrochim. Acta 35, (1990), 1037-1044.

[26] T. Tanaka, A. Nakajima, A. Watanabe, T. Ohno, Y. Ozaki, Surface-enhanced Raman scattering spectroscopy and density functional theory calculation studies on adsorption of *o*-, *m*-, and *p*-nitroaniline on silver and gold colloid. J. Mol. Struct. 661-662, (2003), 437-449.

[27] M. Muniz-Miranda, N. Neto, Surface-enhanced Raman scattering of π-conjugated “push-pull” molecules. Part I. *p*-nitroaniline adsorbed on silver nanoparticles. Colloids and Surfaces A: Physicochem. Eng. Aspects 249, (2004), 79-84.

[28] W. Ma, Y. Fang, Experimental (SERS) and theoretical (DFT) studies on the adsorption of *p*-, *m*-, and *o*-nitroaniline on gold nanoparticles. J. Colloid and International Science 303, (2006), 1-8.

[29] W. Ma, Y. Fang, Experimental (FT-IR) and theoretical (DFT) studies on the adsorption behavior of p-nitroaniline (PNA) on gold nanoparticles. J. Nanoparticle Research 8, (2006), 761-767.

[30] L. B. Zhao, X. X. Liu, D. Y. Wu, Oxidative coupling or reductive coupling? Effect of surroundings on the reaction route of the plasmonic photocatalysis of nitroaniline. J. Phys. Chem. C 120, (2016), 1570-1579.

[31] Q. Ding, M. Chen, Y. Fang, Z. Zhang, M. Sun, Plasmon-Driven Diazo Coupling Reactions of p-Nitroaniline via $–NH_2$ or $–NO_2$ in Atmosphere Environment. J. Phys. Chem. C., 121, (2017), 5225-5231.

[32] W. Lin, X. Ren, L. Cui, M. Sun, Electro-optical tuning of plasmon-driven double reduction interface catalysis, Appl. Mater. Today 11, (2018), 189–192.

[33] Jingang Wang, Xijiao Mu, Mengtao Sun, Optical-electrical synergy on electricity manipulating plasmon-drivenphotoelectrical catalysis, Appl. Mater. Today 15, (2019), 305–314.

[34] E. Cao, X. Guo, L. Zhang, Y. Shi, W. Lin, X. Liu, Y. Fang, L. Zhou, Y. Sun, Y. Song, M.T. Sun, Electrooptical synergy on plasmon–exciton-codriven surface reduction reactions, Adv. Mater. Interfaces 4, (2017), 1700869.

[35] W. Lin, Y. Cao, P. Wang, M. Sun, Unified treatment for plasmon-exciton co-driven reduction and oxidation reactions, Langmuir 33, (2017),12102–12107.

[36] W. Lin, E. Cao, L. Zhang, X. Xu, Y. Song, W. Liang, M. Sun, Electrically enhanced hot hole driven oxidation catalysis at the interface of a plasmon-exciton hybrid, Nanoscale 10, (2018), 5482–5488.

[37] W. B. Cai, B. Ren, X. Q. Li, C. X. She, F. M. Liu, X. W. Cai, Z. Q. Tian, Investigation of surface-enhanced Raman scattering from platinum electrodes using a confocal Raman microscope: dependence of surface roughening pretreatment. Surf. Sci. 406, (1998), 9-22.

[38] R. Gómez, J. M. Pérez, J. Solla-Gullón, V. Montiel, A. Aldaz, In Situ Surface Enhanced Raman Spectroscopy on Electrodes with Platinum and Palladium Nanoparticle Ensembles. J. Phys. Chem. B 108 (28), (2004), 9943–9949.

[39] A. López-Cudero, J. Solla-Gullón, E. Herrero, A. Aldaz, J.M. Feliu, CO Electrooxidation on Carbon Supported Platinum Nanoparticles: Effect of Aggregation. J. Electroanal. Chem. 644, (2010), 117−126.

[40] C. M. Sanchez-Sanchez, F. J. Vidal-Iglesias, J. Solla-Gullon, V. Montiel, A. Aldaz, J.M. Feliu, E. Herrero, Scanning Electrochemical Microscopy for Studying Electrocatalysis on Shape-Controlled Gold Nanoparticles and Nanorods. Electrochim. Acta, 55, (2010), 8252−8257.

[41] H. Erikson, A. Sarapuu, K. Tammeveski, J. Solla-Gullon, J.M. Feliu, Shape-Dependent Electrocatalysis: Oxygen Reduction on Carbon-Supported Gold Nanoparticles. ChemElectroChem, 1, (2014), 1338−1347.

[42] M. J. Frisch, et al. Gaussian 03, Revision D.02; Wallingford: CT, (2004).

[43] M. D. Hanwell, D. E. Curtis, D.C. Lonie, T. Vandermeersch, E. Zurek, G. R. Hutchison, Avogadro: An advanced semantic chemical editor, visualization, and analysis platform. J. Cheminformatics (2012), 4:17

[44] M. Muniz-Miranda, pH Dependence of the Surface-Enhanced Raman Scattering of p-Nitroaniline Adsorbed on Silver Sols. J. Raman Spectrosc. 28, (1997), 205−210.

[45] R. Gómez, J. Solla-Gullón, J. M. Pérez, A. Aldaz, Nanoparticles-on-Electrode Approach for in Situ Surface-Enhanced Raman Spectroscopy Studies with Platinum-Group Metals: Examples and Prospects. J. Raman Spectrosc. 36, (2005), 613−622.

[46] R. Gómez, J. Solla-Gullón, J. M. Pérez, A. Aldaz, Surface-Enhanced Raman Spectroscopy Study of Ethylene Adsorbed on a Pt Electrode Decorated with Pt Nanoparticles. ChemPhysChem 6, (2005), 2017−2021.

[47] O. Lugaresi, J.V. Perales-Rondón, A. Minguzzi, J. Solla-Gullón, S. Rondinini, J. M. Feliu, C. M. Sánchez-Sánchez, Rapid Screening of Silver Nanoparticles for the Catalytic Degradation of Chlorinated Pollutants. Water. Appl. Catal. B163, (2015), 554−563.

[48] A. A. Jbarah, R. Holze, A comparative spectroelectrochemical study of the redox, electrochemistry of nitroanilines, J. Solid State Electrochem 10 (2006) 360–372.

[49] M. H. A. Zavar, S. Heydari, G. H. Rounaghi, H. Eshghi, H. Azizi-Toupkanloo, Electrochemical behavior of para-nitroaniline at a new synthetic crown ether-silver nanoparticle modified carbon paste electrode. Anal. Methods, 4, (2012), 953–958.

[50] V. Chis, M.M. Venter, N. Leopold, O. Cozar, Raman, surface-enhanced raman scattering and DFT study of para-nitro-aniline. Vibr. Spectrosc, 48, (2008), 210-214.

[51] C. D. Lindstrom, X. Y. Zhu, Photoinduced Electron Transfer at Molecule−Metal Interfaces. Chem. Rev. 106, (2006), 4281−4300

[52] M. Zeng, Y. Li, Recent advances in heterogeneous electrocatalysts for the hydrogen evolution reaction, J. Mater. Chem. A 3, (2015), 14942-14962.

[53] Z. W. Seh, J. Kibsgaard, C. F. Dickens, I. Chorkendorff, J. K. Nørskov, T. F. Jaramillo, Combining theory and experiment in electrocatalysis: Insights into materials design, Science 355, (2017), 6321.

[54] P. Quaino, F. Juarez, E. Santos, W. Schmickler, Volcano plots in hydrogen electrocatalysis – uses and abuses, Beilstein J. Nanotechnol. 5, (2014), 846–854

[55] J. J. Chen, J. C. S. Wu, P. C. Wu, D. P. Tsai, Plasmonic photocatalyst for H_2 evolution in photocatalytic water splitting. J. Phys. Chem. C 115(1), (2011), 210-216.

[56] K. Qian, B. C. Sweeny, A. C. Johnston-Peck, W. Niu, J. O. Graham, J. S. DuChene, J. Qiu, Y. C. Wang, M. H. Engelhard, D. Su, E. A. Stach, W. D. Wei, Surface plasmon-driven water reduction: Gold nanoparticle size matters. J. Am. Chem. Soc. 136, (2014), 9842-9845.

[57] B. Wu, D. Liu, S. Mubeen, T. T. Chuong, M. Moskovits, G. D. Stucky, Anisotropic Growth of TiO_2 onto Gold Nanorods for Plasmon-Enhanced Hydrogen Production from Water Reduction. J. Am. Chem. Soc. 138(4), (2016), 1114-1117.

[58] L. Brus, Noble Metal Nanocrystals: Plasmon Electron Transfer Photochemistry and Single-Molecule Raman Spectroscopy. Acc. Chem. Res. 41, (2008), 1742−1749.

[59] L. B. Zhao, Y. F. Huang, X. M. Liu, J. R. Anema, D. Y. Wu, B. Ren, Z. Q. Tian, A DFT study on photoinduced surface catalytic coupling reactions on nanostructured silver: Selective formation of azobenzene derivatives from para-substituted nitrobenzene and aniline. Phys. Chem. Chem. Phys. 14(37), (2012), 12919-12929.

[60] Y. F. Huang, M. Zhang, L. B. Zhao, J. M. Feng, D. Y. Wu, B. Ren, Z. Q. Tian, Activation of oxygen on gold and silver nanoparticles assisted by surface plasmon resonances. Angew. Chem., Int. Ed. 53(9), (2014), 2353-2357.

[61] J. Kaur, R. Singh, B. Pal, Influence of coinage and platinum group metal co-catalysis for the photocatalytic reduction of *m*-dinitrobenzene by P25 and rutile TiO_2. J. Mol. Catal A: Chem. 397, (2015), 99-105.

Figure captions

Figure 1. Representative TEM images of the (a) AgNPs and (a) PtNPs used in this work.

Figure 2. Cyclic voltammograms corresponding to (a) Pt and (b) Ag bead electrodes in 0.1 M $KClO_4$ in the absence (black lines) and presence (red lines) of 1 mM PNA. Scan rate 50 $mV \cdot s^{-1}$. For the sake of clarity (c) represents a zoomed image of (b).

Figure 3. (a) Raman spectrum of solid PNA, (b-f) SERS spectra of PNA adsorbed on Ag in solution (free oxygen environment) at different electrode potentials (from -0.2 V to -0.6 V). Laser of 532 nm. Solution 0.1 M $KClO_4$ + 1mM PNA.

Figure 4. SERS spectra of: (a) adsorbed DAAB on Ag in solution, (b) adsorbed PNA on Ag in solution (free oxygen environment) at -0.2 V and (c) adsorbed PNA on Ag in the presence of O_2 (air environment). Laser of 532 nm. Solution 0.1 M $KClO_4$ + 1mM PNA

Figure 5. Calculated Raman spectra of: (a) DNAB, (b) NAAB and (c) DAAB. SERS spectra of: (d) adsorbed DAAB on Ag in solution, (e) adsorbed PNA on Ag in solution at -0.2 V (free oxygen environment) and (f) adsorbed PNA on Ag in presence of O_2 (air environment).

Figure 6. (a) Raman spectrum of solid PNA. SERS spectra of: (b) adsorbed DAAB on Pt in solution, (c) adsorbed PNA on Pt in the presence of O_2 (air environment), (d-g) adsorbed PNA on Pt in solution (free oxygen environment) at different electrode potentials (from -0.2 V to -0.6 V). Laser of 632.8 nm. Solution 0.1 M $KClO_4$ + 1mM PNA

Figure 7. HOMO and LUMO calculated energy levels of adsorbed PNA and LUMO levels of adsorbed H_2O and O_2 on Pt. Fermi level (EF) of Pt taken from reference [61].

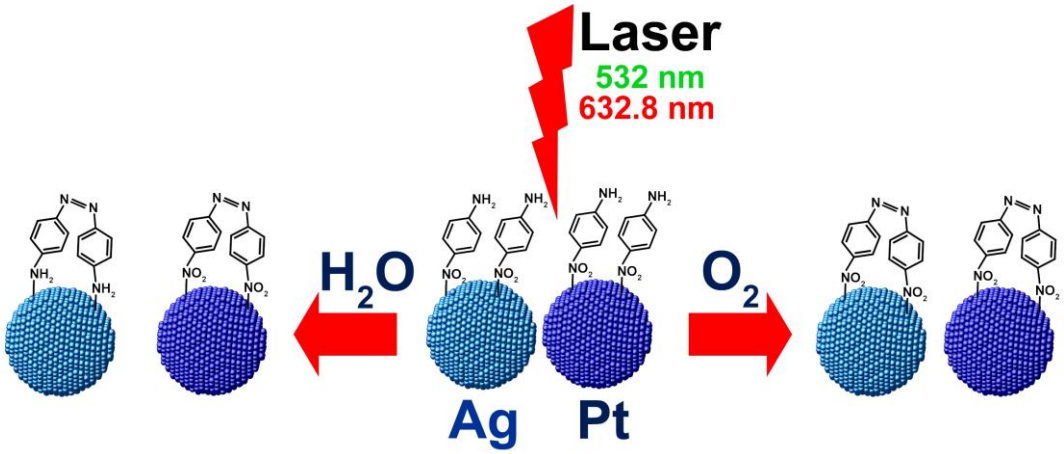

Graphical abstract